Journal of Materials Chemistry A

Accepted Manuscript

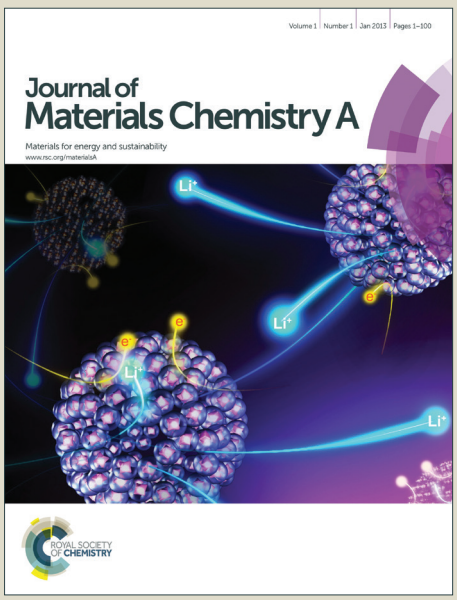

ROYAL SOCIETY OF CHEMISTRY

www.rsc.org/materialsA

Journal of Materials Chemistry A RSCPublishing

ARTICLE

Cite this: DOI: 10.1039/x0xx00000x

One-pot synthesis of yolk–shell mesoporous carbon spheres with high magnetisation

Received 00th April 2014,
Accepted 00th April 2014

DOI: 10.1039/x0xx00000x

www.rsc.org/

Wen-jing Liu[a], Yu-xin Liu[b], Xiang-yang Yan[a], Guo-ping Yong[a], Ye-ping Xu[b], Shao-min Liu*[,a]

A simple and a novel route for the synthesis of monodisperse yolk–shell magnetic mesoporous carbon spheres (Fe_3O_4@void@C) via a 'one-pot' strategy for direct carbonisation and etching was developed. The synthesised materials were characterised by XRD, TEM, SEM, FT-IR, EDS, TGA, N_2 sorption, and magnetic susceptibility measurements, and the ideal conditions for the synthesis of the Fe_3O_4@void@C spheres were systematically investigated. The morphologies and the saturation magnetisation values were observed to be strongly influenced by the composition of the solvent (ethanol:water) and the proportions of TEOS and formaldehyde used in the synthesis. The synthesised materials possessed a large average pore diameter (4.5 nm) and a magnetisation strength (62 emu g^{-1}) greater than that of Fe_3O_4 itself. The performance of Fe_3O_4@void@C in the adsorption of pyrene was tested in aqueous solution, and fast adsorption rates (approximately 40 min to reach equilibrium) and high adsorption capacities (77.1 mg g^{-1}) were observed. In addition, Fe_3O_4@void@C exhibited excellent reusability for the adsorption of pyrene over six adsorption–desorption cycles.

Introduction

In the past few decades, much scientific effort has been directed towards the design and fabrication of nanomaterials with controlled morphologies and tailored properties. As an important family of nanocomposites, mesoporous carbon nanomaterials have attracted increasing attention because of their high surface areas, chemical inertness, biocompatibility, thermal stability, and electrical conductivity. Thus, they have numerous potential applications as catalyst supports,[1,2] adsorbents,[3,4] drug delivery agents,[5,6,7] lithium-ion batteries,[8,9,10] and supercapacitors.[11] However, the extraction of carbon powders from solutions is difficult.[12,13] In particular, the conventional approach is rather time-consuming and expensive, so the development of functional mesoporous carbon with additional physicochemical properties could simplify the separation process.

Magnetic nanocomposites have fascinated scientists for a long time because of their unique qualities, which include well-defined mesoporous structures, unique shapes, and tailored properties. In addition, the separation of mesoporous carbon or silica from magnetic nanocomposite working systems is easy. They are widely used as contrast agents for magnetic resonance imaging, in magnetic storage media, and in magnetic fluids. Coatings with polymer, silica, carbon, or other materials over the magnetic particles can stabilise the naked magnetic nanoparticles against degradation, prevent aggregation, and further functionalise the magnetic nanoparticles to extend their applications in catalysis and biomedicine.

Magnetic mesoporous nanoparticles can be broadly categorised into four types according to their different morphologies, structures, and particle sizes:[14] monodisperse magnetic nanocrystals embedded in mesoporous nanospheres, microspheres encapsulating magnetic cores in a mesoporous shell, mesoporous materials loaded with magnetic nanoparticles inside the porous channels or cages, and rattle-type (or yolk–shell) magnetic nanocomposites. As for magnetic nanocomposites with core–shell structures, their magnetic properties are sometimes restrained to a specific range because the core materials are easily and compactly encapsulated in the shell material. The use of magnetic nanocomposites with a yolk–shell mesoporous structure can be an effective solution to this problem,[15,16] because materials with this unique structure, i.e., with interstitial spaces between the mesoporous shells and the magnetic cores, can have movable magnetic nanoparticles packed in the mesoporous hollow shells. Because the large cavity volume between the yolk and shell provides sufficient space for the loading of drugs,[17] magnetic mesoporous carbon hollow nanoparticles can be used as drug delivery carriers and diagnostic agents for cancer. In addition, further investigations into their applications in catalysis, chemical sensing, lithium-ion batteries,[18] separation membranes, and water-treatment adsorbents have been reported.

The conventional methodology for the synthesis of yolk–shell magnetic carbon includes the use of presynthesised core materials, which are first coated with one or two layers of

different materials. The inner layer of the two shells, or part of the core (shell), is selectively removed by dissolution using a solvent or by calcination. So far, researchers have synthesised four types of yolk–shell nanoparticles: those with single cores, multiple cores, multiple shells, and raspberry-like cores.[19] Zhang and Jiang synthesised yolk–shell magnetic mesoporous carbon using Fe_3O_4@nSiO_2@mSiO_2 microspheres impregnated with a carbon precursor as templates.[20] A surface-modified interior cavity and a magnetic Fe_3O_4–C double-layered shell was also synthesised.[21] Moreover, the authors prepared yolk–shell Fe_3O_4@C mesoporous composites using a nanocasting technology that involved infiltration sucrose and sulphuric acid into mesoporous Fe_3O_4@SiO_2@polymer microspheres, followed by carbonisation and etching processes.[22] Nevertheless, this multistep hard-template approach is time-consuming and expensive. Consequently, a simple procedure for synthesising rattle-type magnetic mesoporous carbon is much in demand for practical applications.

In this paper, we propose a new route for the synthesis of yolk-shell magnetic mesoporous carbon spheres (Fe_3O_4@void@C) with a magnetic Fe_3O_4 particle as the core and a mesoporous carbon layer as the shell. The route is based on a 'one-pot' strategy for carrying out direct carbonisation and etching processes. The effect of the composition of the solvent and proportions of tetraethoxysilane (TEOS) and formaldehyde on the properties of the Fe_3O_4@void@C were intensively investigated, and the pyrene-adsorption performance of the Fe_3O_4@void@C nanocomposites was also investigated.

Experiments

Materials and chemicals

Pyrene was purchased from Sigma-Aldrich. HPLC-grade acetonitrile was obtained from Thermo Fisher Scientific Corp. (Fair Lawn, NJ, USA). Trisodium citrate (Na_3Cit), anhydrous $FeCl_3$, sodium acetate (NaAc), ethylene glycol, ammonium hydroxide (28%), TEOS, resorcinol, formaldehyde (37.0%–40.0%), ethanol, and sodium hydroxide (NaOH) were of analytical grade and purchased from Sinopharm Shanghai Chemical Corp. (China). All reagents were used without further purification. Doubly distilled water obtained from a laboratory purification system was used throughout the experiments.

Synthesis

Procedure for the preparation of Fe_3O_4 nanospheres. Fe_3O_4 particles were synthesised in accordance with the previously reported method.[23] $FeCl_3$ (3.0 g) and Na_3Cit (0.83 g) were dissolved in 100 mL of ethylene glycol, and NaAc (4.8 g) was subsequently added with magnetic stirring. After it was stirred vigorously for 30 min, the yellow solution was sealed in a 100-mL capacity Teflon-lined stainless-steel autoclave. The autoclave was heated to 200 °C, maintained at this temperature for 10 h, and then allowed to cool to room temperature. The final black product was washed successively with ethanol and doubly distilled water several times and was finally dried at 60 °C for 8 h.

Procedure for the preparation of Fe_3O_4@polymer, Fe_3O_4@C, and Fe_3O_4@void@C. A mixture consisting of 0.25 g of Fe_3O_4 nanospheres, 150 mL of ethanol, and 50 mL of H_2O was ultrasonicated for 10 min and then injected into a 250-mL three-necked round-bottom flask. Next, 0.3 g of resorcinol and 3.9 mL of 28% $NH_3 \cdot H_2O$ were added, and the mixture was mechanically stirred for 1 h at 30 °C. Then, 0.45 mL of formaldehyde solution was added dropwise, followed by the dropwise addition of 0.62 mL of TEOS, and the mixture was stirred for 6 h. The mixture was subsequently heated at 80 °C for 8 h under stirring. The resultant solid product was filtered, washed, and subsequently dried at 60 °C for 12 h. The obtained sample is denoted as Fe_3O_4@polymer. For the carbonisation process, the Fe_3O_4@polymer nanospheres were heated under a N_2 atmosphere to 600 °C at a heating rate of 1 °C min^{-1} and were maintained at 600 °C for 3 h (denoted as Fe_3O_4@SiO_2·C). The Fe_3O_4@SiO_2·C was subsequently etched with 10 mol L^{-1} NaOH for 12 h at room temperature, and the products were successively washed with doubly distilled water and ethanol several times. The obtained sample is denoted as Fe_3O_4@void@C. For comparison, Fe_3O_4@C was prepared using the same methods and synthetic conditions previously described, except that TEOS was not added.[24]

Characterisation

Scanning electron microscopy (SEM) images were recorded on a Philips XL30 electron microscope (Netherlands) operated at 20 kV. A thin gold film was sprayed onto each sample before it was inserted into the instrument. Transmission electron microscopy (TEM) images were collected using a JEOL 2010 electron microscope operated at 200 kV. FT-IR spectra were recorded on a Brock Tensor 27 Fourier-transform infrared spectrometer after the samples were combined with KBr and compacted into tablets. Powder X-ray diffraction (PXRD) patterns of the samples were recorded on a Philips X′Pert PRO SUPER diffractometer equipped with a nickel-filtered Cu-Kα radiation source (λ = 1.540598 Å) operated at 40 kV and 200 mA. Thermogravimetric analysis (TGA) was performed on a Mettler Toledo TGA-SDTA851 analyser (Switzerland) over the temperature range 25–800 °C at a heating rate of 5 °C min^{-1} and under flowing N_2 (80 mL min^{-1}). Magnetic characterisation was performed on a superconducting quantum interference device (SQUID) magnetometer. Nitrogen sorption isotherms were measured at 77 K using a Micromeritics Tristar 3000 analyser. The Brunauer–Emmett–Teller method was utilised to calculate the specific surface areas. The pore volumes and pore size distributions were determined according to the Barrett–Joyner–Halenda model using the desorption branches of the isotherms, and the total pore volumes were estimated from the adsorbed amount at a relative pressure P/P_0 of 0.999.

Application of mesoporous Fe_3O_4@void@C nanospheres for the adsorption of pyrene in aqueous solution and the reuse of Fe_3O_4@void@C

A pyrene stock solution (200 μg mL^{-1}) was prepared by dissolving 50 mg of pyrene in 250 mL of doubly distilled water. In the adsorption experiments, 10 mg of magnetic Fe_3O_4@void@C or Fe_3O_4@SiO_2·C adsorbent was suspended in 500 mL of pyrene water solution with a pyrene concentration between 0.3 μg mL^{-1} and 1.6 μg mL^{-1}. The resulting mixture was shaken at room temperature for 5 h. After magnetic separation using an external magnet in the case of the Fe_3O_4@void@C nanosphere samples, the equilibrium concentrations of pyrene were measured by high-performance liquid chromatography with fluorescence detection (HPLC-FLD, Agilent 1100) using an excitation wavelength of λ_{ex} = 295 nm and an emission wavelength of λ_{em} = 406 nm.

Approximately 50 mg of Fe_3O_4@void@C particles was suspended in 500 mL of aqueous solution with a pyrene concentration of 1.0 μg mL^{-1}. The adsorption process was subsequently performed as previously described. After the adsorption process, the material was washed three times with methanol and then dried at 60 °C until a constant weight was reached. This adsorption and desorption procedure was repeated six times.

Results and discussion

Preparation of yolk–shell magnetic mesoporous carbon composite spheres

Scheme 1 shows the preparation of yolk–shell magnetic mesoporous carbon composite spheres. First, Fe_3O_4 magnetic nanoparticles were prepared using a solvothermal method.[23] The hydrolysis and polymerisation of TEOS and the polymerisation of resorcinol and formaldehyde were performed in a round-bottom flask. Because (1) the hydrolysis and polymerisation of TEOS are faster than the polymerisation of resorcinol and formaldehyde and (2) TEOS can inhibit the polymerisation of resorcinol and formaldehyde,[25] the hydrolysis and polymerisation of TEOS was favoured in the early stages of the reaction. Subsequently, $Si(OH)_4$ (the hydrolysis product of TEOS) underwent dehydration in the presence of the phenolic hydroxyl or hydroxyl methyl groups of methylol phenol, and the TEOS reagent interacted with the phenolic resin.[26] As the reaction progressed and the TEOS hydrolysis and polymerisation processes neared completion, the polymerisation of resorcinol and formaldehyde became the predominant process, resulting in the formation of a phenolic resin polymer layer (Fe_3O_4@polymer). Finally, yolk–shell magnetic mesoporous carbon spheres were obtained after the carbonisation and etching processes.

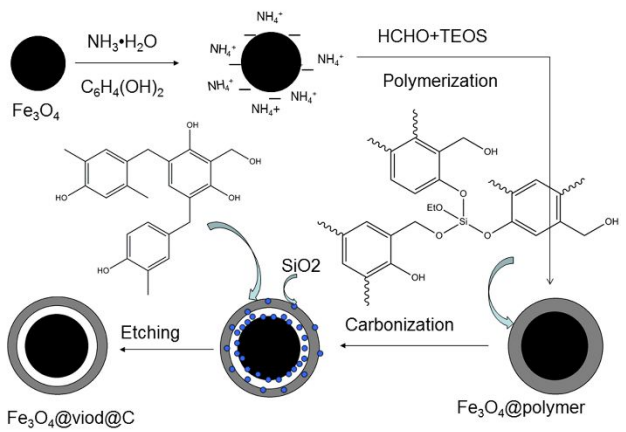

Scheme 1 Possible synthetic mechanism for mesoporous Fe_3O_4@void@C.

The composition of the solvent plays a key role in the formation of the phenolic resin–TEOS polymer. After performing a series of optimisation experiments (ethanol:water = 0:1, 1:1, 2:1, 2.5:1, 3:1, 4:1, 7:1, and 1:0), we determined that the optimum solvent composition for achieving the best dispersity and morphology of Fe_3O_4@polymer is ethanol:water = 2.5:1–4:1 (Fig. S1, ESI†). The synthesis of the core–shell-structured Fe_3O_4@polymer in a solvent with a low ethanol concentration is difficult. However, because hydroxyl hydrolytic polymerisation occurs during the whole polymerisation process, polymer adhesion easily occurs in pure ethanol. Thus, the concentration of ethanol in the solvent must not be too high.

More importantly, the TEOS content directly affects the morphology of the cavities and the sizes of the pores after etching. Therefore, the molar proportion of TEOS is the key factor governing the structure of mesoporous Fe_3O_4@void@C. We synthesised magnetic mesoporous carbon using a certain quantity of Fe_3O_4 and various TEOS:formaldehyde proportions to obtain mesoporous materials with different properties. We can draw a few conclusions from the supplementary information in Fig. S2 (ESI†). When the TEOS content was zero, the yolk–shell structure could obviously not be formed. As the amount of TEOS was gradually increased, the final magnetic materials started to form cavities consistent with the yolk–shell structure after etching only when the HCHO:TEOS proportion reached 1:1. Fe_3O_4 could not be encapsulated in a polymer layer when the HCHO:TEOS ratio was 1:5, further illustrating that TEOS inhibits the polymerisation of resorcinol and formaldehyde. In the syntheses with HCHO:TEOS = 0:1, we only obtained Fe_3O_4 after etching when the outer package material was pure SiO_2.

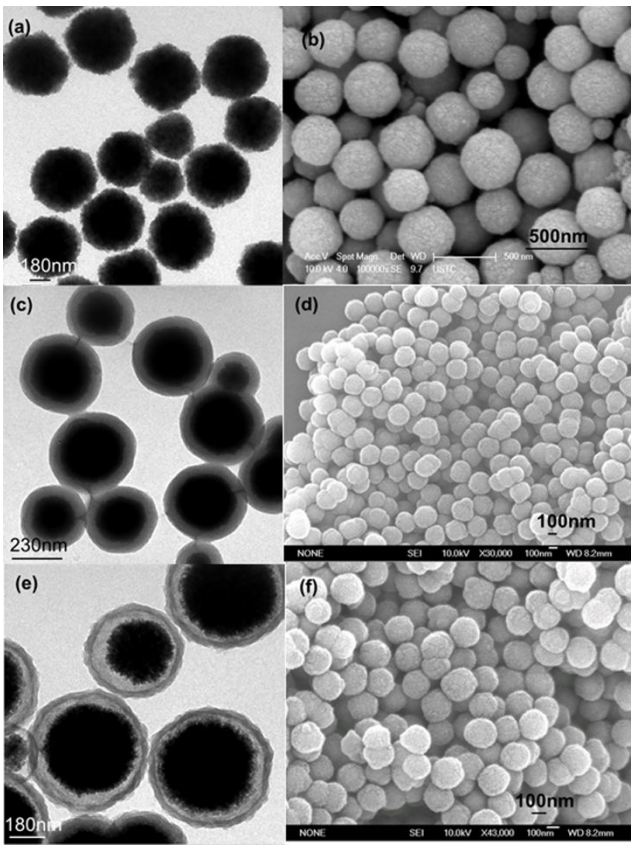

Fig. 1 (**a**, **c**, **e**) TEM and(**b**, **d**, **f**) SEM images of (**a**, **b**) Fe_3O_4 spheres, (**c**, **d**) Fe_3O_4@polymer, and (**e**, **f**) Fe_3O_4@void@C mesoporous spheres.

Table 1 Effects of precursor material dosage on the shell thickness of Fe_3O_4@polymer spheres.

Fe_3O_4 spheres (g)	Resorcinol (g)	Formaldehyde solution (mL)	TEOS (mL)	Shell thickness (nm)
0.25	0.2	0.3	0.41	40
0.25	0.3	0.45	0.62	60
0.25	0.4	0.6	0.82	80

When the amount of Fe_3O_4 nanospheres in the previously discussed reaction system was kept constant, the thickness of the shells could be tuned between 40 and 80 nm. In addition, the thickness gradually increased with increasing amounts of resorcinol, formaldehyde, and TEOS (Table 1). Furthermore, the shells remained highly uniform and monodisperse. These results indicate that the mesoporous carbon shell thickness of Fe_3O_4@void@C can be easily adjusted by changing the amount of polymer precursor used. A TEM image of this material is provided in Fig. S3 (ESI†).

Characterisation of Fe_3O_4@void@C

The morphology of the obtained nanoparticles was characterised by SEM and TEM. Fig. 1 presents representative SEM and TEM images of the obtained Fe_3O_4, Fe_3O_4@polymer, and Fe_3O_4@void@C mesoporous nanospheres. Figs. 1a and 1b show that the Fe_3O_4 nanospheres are highly monodisperse and spherical with a smooth surface and an average diameter of 200 nm. This is likely because Fe_3O_4 cores whose surfaces are decorated with citric acid anions facilitate the formation of the phenolic resin polymer and SiO_2.[21] The formation of a uniform polymer shell around the Fe_3O_4 cores is evident in Figs. 1c and d. The encapsulated nanoparticles are uniform and monodisperse in solution, and the thickness of the polymer shells is approximately 60 nm. Because (1) the polymerised shells outside of the Fe_3O_4 spheres are covalently bonded three-dimensional polymer frameworks and (2) the high-temperature treatment at 600 °C under the N_2 atmosphere only serves to carbonise the polymer into carbon, the morphology of the obtained Fe_3O_4@SiO_2·C does not undergo a transformation, and the particles are more monodisperse and uniform than in samples prepared using common methods. Figs. 1e and 1f show the nanoparticles with yolk–shell structures after etching with NaOH (10 mol L^{-1}), where the centres are the magnetic cores and the outer layers are mesoporous carbon materials. The shells are composed of a dark-contrast inner layer and a light-contrast outer layer, which are attributed to the Fe_3O_4 and carbon components, respectively. Clearly, the outer carbon layer can protect the inner magnetic shell from the outside environment. As is evident in Figs. 1e and 1f, the nanoparticles exhibit good dispersibility, which prevents the decrease in adsorption efficiency caused by agglomeration.

Fig. 2 shows the wide-angle XRD patterns of the Fe_3O_4 and mesoporous Fe_3O_4@void@C samples. The peaks at $2\theta = 30.3°$, 35.6°, 43.3°, 53.7°, 57.5°, and 62.9° can be assigned as the (220), (311), (400), (422), (511), and (440) characteristic diffraction peaks of the Fe_3O_4 nanoparticles, respectively (JCPDS no. 19-629). The intensities of the diffraction peaks of Fe_3O_4 for the Fe_3O_4@void@C sample are stronger than those for the Fe_3O_4 sample, and the diffraction peaks are narrow. Furthermore, the (111) and (222) planes of Fe_3O_4 also appear in the pattern of the Fe_3O_4@void@C sample.

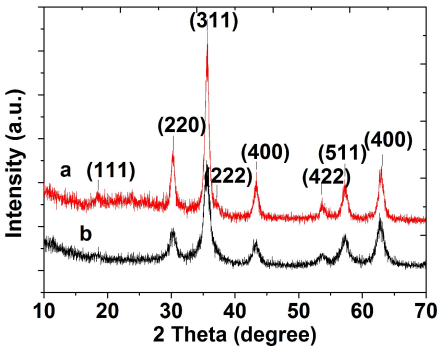

Fig. 2 Wide-angle XRD patterns of (**b**) Fe_3O_4 nanoparticles and (**a**) mesoporous Fe_3O_4@void@C spheres.

The EDS pattern reveals that the Fe_3O_4@polymer contains Si, Fe, and C (Fig. S4, ESI†), indicating that the Fe_3O_4@polymer materials contain Si. Moreover, the FT-IR spectra of the three materials (Fe_3O_4@polymer, Fe_3O_4@SiO_2·C, and Fe_3O_4@void@C) exhibit a strong and wide absorption band at 1089 cm^{-1}, which is attributable to Si—O—Si stretching vibrations, and absorption bands at 796 cm^{-1} and 471 cm^{-1}, which are assigned to Si—O symmetric stretching vibrations. Notably, the broad band at 3450 cm^{-1} is an antisymmetric stretching vibration of constitutional water, and the peak at approximately 1638 cm^{-1} is attributed to the bending vibration of water. Moreover, the weak peak at 960 cm^{-1} is attributable to bending vibrations of the Si—O bonds. The FT-IR spectra in Figs. 3a and 3c indicate that the signals associated with Si—O—Si bonds become more intense after high-temperature calcination of the magnetic carbon material, and the spectrum in Fig. 3b contains no signal related to Si—O—Si bonds. We conclude that SiO_2 was completely removed by the NaOH (10 mol L^{-1}) etching process.

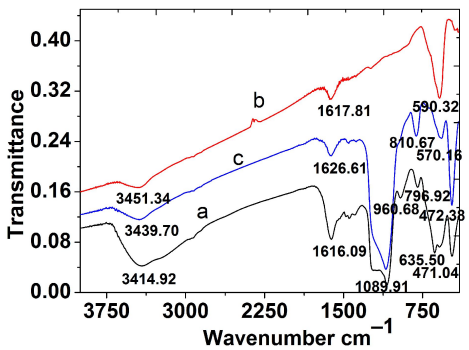

Fig. 3 FT-IR spectra of (**a**) Fe_3O_4@polymer, (**b**) Fe_3O_4@SiO_2·C, and (**c**) mesoporous Fe_3O_4@void@C spheres.

The specific surface areas of the Fe_3O_4@void@C samples with shell thicknesses of 40, 60, and 80 nm (hereafter, called the Fe_3O_4@void@C-40, -60, and -80 samples respectively) and of the Fe_3O_4@SiO_2·C-60 sample are 138.0 m^2 g^{-1}, 235 m^2 g^{-1}, 277 m^2 g^{-1}, and 111.6 m^2 g^{-1}, respectively. The N_2 adsorption and desorption curves are presented in Fig. S6a (ESI†), and the pore size distribution curve is presented in Fig. S6b (ESI†). The typical type-VI N_2 adsorption and desorption curves of Fe_3O_4@void@C demonstrate that this material is a typical mesoporous material. The results also demonstrate that the specific surface area of the yolk–shell composite spheres is greater than that of the Fe_3O_4@C microspheres. However,

compared with carbon materials directly synthesised using the extended Stöber method[19] in the absence of TEOS, the magnetic carbon material with the (Fe_3O_4@void@C-60) prepared in this work is obviously more mesoporous, as shown in Fig. 4. Furthermore, the Fe_3O_4@void@C-60 reaches saturation adsorption at P/P_0 = 0.999 (Fig. 4a) and exhibits an average pore diameter of 4.5 nm (Fig. 4b), which is larger than that of the Fe_3O_4@C microspheres, 3.8 nm. The Fe_3O_4@void@C-60 also exhibits a narrow pore size distribution, whereas the Fe_3O_4@C exhibits wide pore diameter distribution.

The TGA curves (Fig. S5, ESI†) recorded under N_2 demonstrate the stability of the mesoporous nanosphere materials after calcination at 600 °C in nitrogen and their high degree of carbonisation.

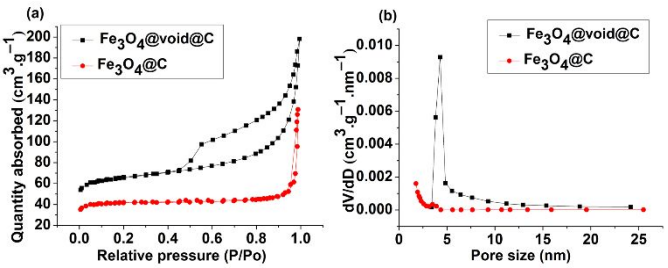

Fig. 4 (**a**) N_2 sorption-desorption curves and (**b**) pore diameter distribution curves.

The magnetic hysteresis curves obtained at room temperature (Fig. 5) show that Fe_3O_4 exhibits a magnetic susceptibility of 55 emu g^{-1}. Different shell thicknesses in the Fe_3O_4@void@C materials led to obvious differences in their magnetic properties. The magnetic susceptibilities of the magnetic mesoporous carbon materials with shell thicknesses of 40 nm and 80 nm were 50 emu g^{-1} and 42 emu g^{-1}, respectively. However, the magnetic susceptibility of the magnetic mesoporous carbon material with a 60-nm shell thickness was 62 emu g^{-1}, which is higher than the magnetic susceptibility of Fe_3O_4 itself. The reasons for this behaviour are not clear and require further research. Nevertheless, the strong magnetic properties of these materials are advantageous for their use as magnetic separators.

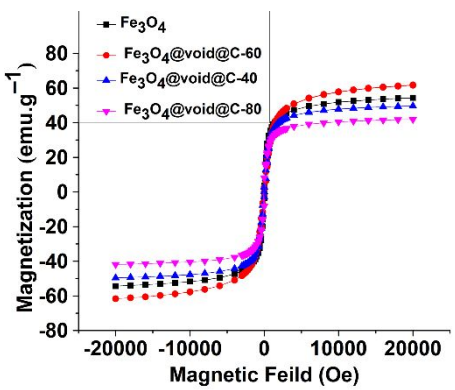

Fig. 5 Magnetization curves for Fe_3O_4 and Fe_3O_4@void@C materials with different shell thicknesses.

Adsorption and separation behaviour and reusability of Fe_3O_4@void@C

Currently, magnetically separable mesoporous carbon materials are highly attractive for the adsorption and enrichment of organic pollutants.[27] For example, polycyclic aromatic hydrocarbons (PAHs) are priority pollutants that have been widely distributed in our environment and exhibit toxic, carcinogenic, and mutagenic properties. In this study, pyrene was chosen as a model PAH pollutant, and the adsorption of pyrene on Fe_3O_4@void@C samples in water was investigated. Fig. 6a presents the adsorption kinetics of Fe_3O_4@void@C-60 as a pyrene absorbent. Clearly, Fe_3O_4@void@C exhibits moderate adsorption rates for pyrene, and it reaches absorption equilibrium within 40 min, which is a short time compared with that required by active carbon (approximately 6 h).[28] The isotherms for pyrene adsorption of onto Fe_3O_4@void@C samples with different shell thicknesses in water are provided in Fig. 6b. Fe_3O_4@void@C-60 exhibited the largest adsorption capacity of 77.1 mg g^{-1}, followed by Fe_3O_4@void@C-40 (70.0 mg g^{-1}) and Fe_3O_4@void@C-80 (48.2 mg g^{-1}). Fe_3O_4@void@C-80 possesses the thickest shell, but its adsorption capacity was not the largest among the investigated samples. The thick carbon layer prevents the pyrene from accessing the cavities, because this mesoporous carbon does not exhibit a highly ordered structure conducive to adsorption. This lack of order reduces the storage capacity of the cavities for pyrene. In contrast, the carbon content of Fe_3O_4@void@C-40 is too low. Thus, only Fe_3O_4@void@C-60 has sufficient carbon outside the Fe_3O_4 core, and this material is likely to have a greater cavity capacity than Fe_3O_4@void@C-40 and Fe_3O_4@void@C-80. Fe_3O_4@SiO_2·C exhibits an adsorption capacity substantially lower than that of Fe_3O_4@void@C, although they have the same carbon thickness. This result may indicate that the cavity in the Fe_3O_4@void@C yolk–shell structure can store a portion of the target species.

In summary, the yolk–shell-structured material exhibits superior adsorption performance compared with pure mesoporous carbon. Furthermore, the shell thickness of the yolk–shell-structured materials strongly influences their adsorption performance. Fe_3O_4@void@C-60 exhibits the best performance among the investigated materials for the adsorption of pyrene in aqueous solution.

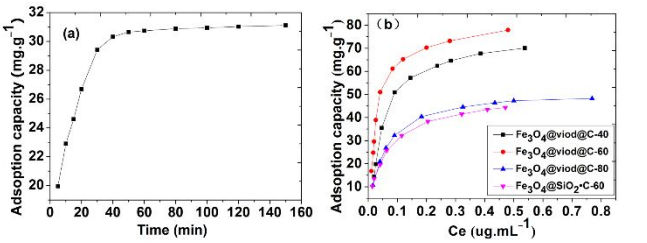

Fig. 6 (**a**) Adsorption kinetics and (**b**) adsorption isotherms of Fe_3O_4@void@C with different shell thicknesses and Fe_3O_4@SiO_2·C with a shell thickness of 60 nm in aqueous solution.

The sorption and desorption cycle was repeated six times using the same Fe_3O_4@void@C sample to evaluate its reusability. The results in Fig. 7 show that the recovery of pyrene remains greater than 84% over the six cycles, indicating that Fe_3O_4@void@C is reusable after being regenerated.

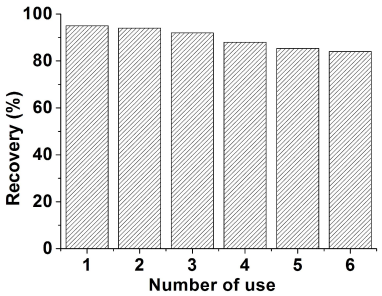

Fig. 7 Reuse results for Fe_3O_4@viod@C over six cycles

Table 2 compares the adsorption performance of the obtained Fe_3O_4@void@C with the performance of other adsorbents reported previously. It is clear that the prepared Fe_3O_4@void@C materials have the highest saturation magnetization among the various magnetic adsorbents and a higher adsorption capacity than multiwalled carbon nanotubes, mesoporous polysilsesquioxane, and SiO_2/Fe_3O_4-C. This might be due to the unique yolk–shell structure and good dispersibility of the material. In particular, this structure is helpful for the synthesis of strong magnetic core-shell materials and for increasing the adsorption capacity.

Table 2 Comparison of the adsorption properties of pyrene on various adsorbents.

Adsorbents	Morphology of adsorbents	Adsorption capacity (mg g−1)	Magnetism (emu g−1)	ref
Multiwalled carbon nanotubes	Long tube	42.7	-	29
Activated carbon	reticular	147.6	-	30
mesoporous polysilsesquioxane	cubic	38.0	-	31
SiO2/Fe3O4 - C	rattle	41.5	29.5	21
SiO2/Fe3O4 - C/C18	rattle	175	22.8	21
Yolk-shell magnetic mesoporous carbon	Yolk-shell	77.1	62	This work

Conclusions

In summary, we have developed a facile method for the preparation of monodisperse yolk–shell mesoporous carbon spheres by carbonising Fe_3O_4@polymer materials synthesised using resorcinol, formaldehyde, and TEOS. After the SiO_2 was removed, the obtained Fe_3O_4@void@C mesoporous nanospheres exhibited a magnetic susceptibility (62 emu g^{-1}) greater than those of samples obtained using other common methods, which further accelerates its magnetic separation in aqueous solutions. Preliminary investigations demonstrated that these mesoporous Fe_3O_4@void@C composite spheres possess mesopores, are highly stable, and exhibit moderate adsorption and separation behaviours and large and tuneable specific surface areas. In addition, our material can be directly used in water and has a large adsorption capacity. This material effectively avoids incompatibility with various sorbents and simplifies the experimental separation procedure. The Fe_3O_4@void@C also exhibited excellent reusable performance for six pyrene sorption–desorption cycles. Therefore, these yolk–shell magnetic mesoporous carbon spheres have potential uses in numerous applications.

Acknowledgements

We gratefully acknowledge the Commonwealth Scientific Foundation for Industry of Chinese Inspection and Quarantine (No. 201210071) of the Ministry of National Science and Technology of China.

Notes and references

[a]*Department of Chemistry, University of Science and Technology of China, Hefei 230026, P. R. China. Fax&Tel: 0551-63492147; E-mail: liusm@ustc.edu.cn.*
[b]*Technology Center, Anhui Entry-Exit Inspection and Quarantine Bureau, Hefei 230022, P.R. China*

† Electronic Supplementary Information (ESI) available: [EDS, SEM, TEM, N_2 sorption and adsorption curve, pore diameter distribution curve, adsorption isotherms curve, TGA]. See DOI: 10.1039/b000000x/

[1] Y. Liu, L. Zhou, Y. Hu, C. F. Guo, H. S. Qian, F. Zhang, X. W. (David) Lou, *J. Mater. Chem.*, 2011, **21**, 18359.
[2] S. L. Zhang, L. Chen, S. X. Zhou, D. Y. Zhao, L. M. Wu, *Chem. Mater.*, 2010, **22**, 3433.
[3] Y. P. Zhai, Y. Q. Dou, X. X. Liu, B. Tu, D. Y. Zhao, *J. Mater. Chem.*, 2009, **19**, 3292.
[4] D. Saha, S. G. Deng, *Langmuir.*, 2009, **25**, 12550.
[5] A. H. Yan, B. W. Lau, B. S. Weissman, I. Kulaots, N. Y. C. Yang, A. B. Kane, R. H. Hurt, *Adv. Mater.*, 2006, **18** ,2373.
[6] Y. Fang, D. Gu, Y. Zou, Z. X. Wu, F. Y. Li, R. C. Che, Y. H. Deng, B. Tu, D. Y. Zhao, *Angew. Chem, Int. Edit.*, 2010, **49**,7987.
[7] T. W. Kim, P. W. Chung, I. I. Slowing, M. Tsunoda, E. S. Yeung, V. S. Y. Lin, *Nano Lett.*, 2008, **8**, 3724.
[8] Y. G. Guo, Y. S. Hu, J. Maier, *Chem. Commun.*, 2006, **26**, 2783.
[9] J. S. Chen, H. Liu, S. Z. Qiao, X. W. Lou, *J. Mater. Chem.,* 2011, **21**, 5687.
[10] X. W. Lou, D. Deng, J. Y. Lee, L. A. Archer, *Chem. Mater.,* 2008, **20**, 6562 .
[11] H. J. Liu, W. J. Cui, L. H. Jin, C. X. Wang, Y. Y. Xia, *J. Mater. Chem.*, 2009, **19**, 3661.
[12] A. H Lu, W. S chmidt, N. Matoussevitch, H. Bonnemann, B. Spliethoff, B. Tesche, E. Bill, W. Kiefer and F. Schuth, *Angew. Chem. Int. Ed.*, 2004, **43**, 4303.
[13] A. B. Fuertes, P. Tartaj, *Chem. Mater.*, 2006, **18**, 1675.
[14] J. Liu, S. Z. Qiao, Q. H. Hu, G. Q.(Max)Lu, *Wiley-VCH Verlag GmbH, Co. KGaA, Weinheim.*, 2011, **4**, 425.
[15] J. S. Chen, C. M. Li, W. W. Zhou, Q. Y. Yan, L. A. Archer, X. W. Lou, *Nanoscale.*, 2009, **1**, 280 .
[16] X. J. Wu, D. S. Xu, *Adv. Mater.,* 2010, **22**, 1516 .
[17] W. R. Zhao, H. R. Chen, Y. S. L, L. Li, M. D. Lang, J. L. Shi, *Adv. Funct. Mater.*, 2008, **18**, 2780.
[18] S. J. Ding, D. Y. Zhang, H. B. Wu, Z. C. Zhang, X. W. Lou, *Nanoscale*., 2012, **4**, 3651.
[19] J. Liu, S. Z. Qiao, J. S. Chen, X. W. (David) Lou, X. Xing, G. Q. (Max) Lu, *Chem. Commun.*, 2011, **47**, 12578.

[20] X. H. Zhang, L. Jiang, *J. Mater. Chem*., 2011, **21**, 10653.
[21] T. Zeng, X. L. Zhang, Y. R. Ma, S. H. Wang, H. Y. Niu, Y. Q. Cai, *Chem. Commun*., 2013, **49**, 6039.
[22] Y. Y. Yin, S. X. Zhou, C. Min, L. M. Wu, *J. Colloid Interface Sci*., 2011, **361,**527.
[23] J. Liu, Z. K. Sun, Y. H. Deng, Y. Zou, C. Y. Li, X. H. Guo, L. Q. Xiong, Y. Gao, F. Y. Li, D. Y. Zhao, *Angew. Chem*. *Int. Ed*., 2009, **48**, 5875.
[24] X. B. Zhang, H. W Tong, S. M. Liu, G. P. Yong, Y. F .Guan, *J, Mater Chem A.,* 2013, **10**, 1039.
[25] C. L. Chiang, C. C. M. Ma, *Polym. Degrad. Stab.*, 2004, **83(2)**, 207.
[26] C. L. Chiang, C. Chi, M. Ma, *Polym. Degrad. Stab.*, 2004, **83(2)**, 209.
[27] (a) Z. Y. Zhang, J. L. Kong, *J. Hazard.Mater.*, 2011,**193**,325; (b) D. W. Wang, F. Li, G. Q. Lu, H. M. Cheng, *Carbon.*, 2008, **46**, 1593.
[28] B. Cabal, C. O. Ania, J. B. Parra, J. J. Pis, *Chemosphere.*, 2009, **76**, 433
[29] K. Yang, L. Z. Zhu, B. S. Xing, *Environ. Sci. Technol.,* 2006, **40**,1855
[30] F. M. T. Luna, C. C. B. Araújo, C. B. Veloso, I. J. Silva Jr, D. C.S. Azevedo, C. L. Cavalcante Jr, *Adsorption.*, 2011, **17**, 937
[31] D. R. Lin, Q. Zhao, L. J. Hu, B. S. Xing, *chemosphere.*, 2013,**11**,62.

Graphical abstract

One-pot synthesis of yolk–shell mesoporous carbon spheres with high magnetisation

Wen-jing Liu[1], Yu-xin Liu[2], Xiang-yang Yan[1], Guo-ping Yong[1], Ye-ping Xu[2], Shao-min Liu[*,1]

[1]Department of chemistry, University of Science and Technology of China, Hefei, Anhui, 230026, China, Tel&Fax: +86 551 3492147, E-mail: liusm@ustc.edu.cn.

[2]Technology Center, Anhui Entry-Exit Inspection and Quarantine Bureau, Hefei 230022, P.R. China

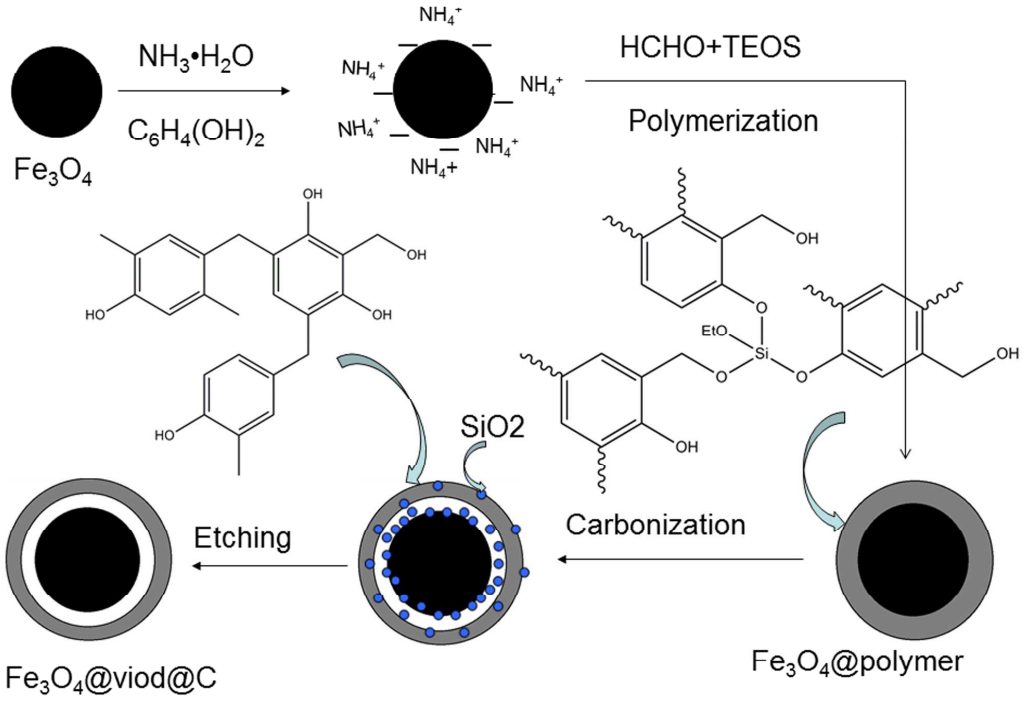

monodisperse yolk-shell magnetic mesoporous carbon spheres（Fe_3O_4@void@C） were obtained by carbonization Fe_3O_4@polymer and etching by NaOH